Simulation of Droplet-based Microfluidics Devices using a Volume of Fluid (VOF) Approach

A. Chandorkar*, S. Palit*

*Flow Science Inc.
683 Harkle Road, Ste A
Santa Fe, NM 87505, USA
Email: shayan@flow3d.com
Phone: 505-982-0088, Fax: 505-982-5551

ABSTRACT

This paper demonstrates that Computational Fluid Dynamics (CFD) simulations can be used to study important physical phenomena in Droplet-based Microfluidics Devices. The Volume of Fluid (**TruVOF**®) method in ***FLOW-3D***® (a general purpose CFD software) has been used to study three devices. The first example is a T-junction where a continuous flow in one channel is sheared off by a dispersion flow in the perpendicular channel. The flow patterns are closely examined and compared with experiments. The second example is a study of a co-flowing device where the formation and breakup of bubbles is simulated. The effect of viscosity on bubble formation is also analyzed. In these two examples the bubble size and frequency are related to important parameters like the width of the channel (w) and the ratio of the flow rates in the two streams (Q_g/Q_l). These relationships are also corroborated with experimental data. The third example is the application of the **TruVOF**® method in predicting phenomena such as electrowetting and electrophoresis. The contact angle is plotted against the voltage applied across a small water droplet on a dielectric material with known properties. The results are compared with the Young-Lippmann curve. The comparisons indicate a good agreement, except at the highest voltages where experiments indicate the presence of saturation effects that limit the reduction in the apparent contact angle.

Keywords: droplet-based microfluidics devices, co-flowing devices, t-junction, electrowetting, volume of fluid method

1 INTRODUCTION

There has been considerable interest in the study of droplet and bubble formation in microfluidic devices in the recent past. This droplet and bubble formation has several applications, for example, on-chip separation, chemical reactions and biochemical synthesis [1]. A related phenomenon that has also garnered much interest recently is electrowetting. This phenomenon can be used to manipulate small liquid droplets on solid surfaces. Applications include Lab on a Chip applications, electronic displays and adjustable lenses [2]. In this paper, the effectiveness of the Volume of Fluid (VOF) method in simulating these processes will be demonstrated. The Volume of Fluid method is a numerical method for accurately tracking and advecting an interface between two fluids [3]. The method deals with the VOF function which measures the fraction of a given fluid in a unit cell. The interface is tracked by solving the kinetic equation for VOF. In the absence of any mass sources this equation is:

$$V_f \frac{\partial F}{\partial t} + \nabla \cdot (AUF) = 0 \qquad (1)$$

Here $A = (A_x, A_y, A_z)$ and V_f represent the area fractions and the volume fraction of the geometrical constraints of the flow. U is the velocity vector and AU is the vector $(A_x u, A_y v, A_z w)$. In this paper, simulations were run using the **TruVOF**® method used in ***FLOW-3D***®, a commercial CFD software. The **TruVOF**® method in ***FLOW-3D***® has several enhancements over the standard VOF method, which improve the general accuracy and stability of the algorithm. In the following section, the simulation results obtained for two microfluidic devices, i.e., the T-junction and the co-flowing device will be summarized. The simulation results obtained for a simple electrowetting case will also be discussed.

2 T-JUNCTION

In a T-junction, the disperse phase and the continuous phase are injected from the two branches of a "T". It is one of the most widely-used devices that produces immiscible droplets.

2.1 T-junction simulation setup

The simulation setup consists of a T-junction with 50µm x 50µm micro channels. Figure 1 shows a schematic of the simulation setup. Here water is the disperse phase and a perfluorocarbon, PFD is the continuous phase. Each simulation computed 24ms of physical time which allowed sufficient time for the formation of several droplets along the channel length.

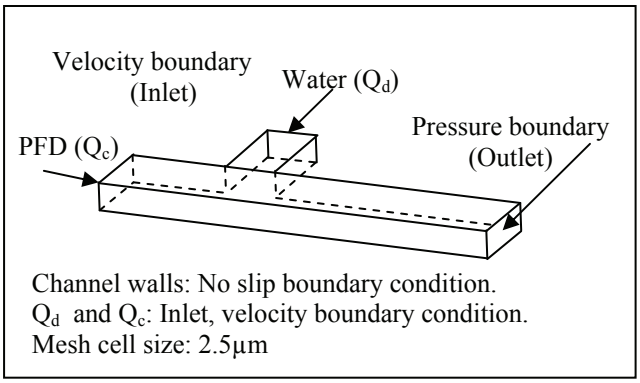

Figure 1: T-junction simulation setup.

2.2 Results and discussions

First the accuracy of the **TruVOF**® method in capturing the droplet formation process was validated. This was done for a case with the continuous phase flow rate, Q_c = 3.6µl/min and discrete phase flow rate of Q_d = 3.9µl/min. Figure 2 shows a comparison of simulation results against the experimental results [4] for this case.

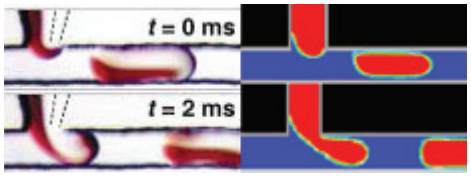

Figure 2: Comparison of ***FLOW-3D***®results with the experimental results.

The effect of the Q_d/Q_c ratio on droplet length and frequency was then studied. Several simulations were run for the geometry described above by changing the continuous phase flow rate while keeping the discrete phase flow rate constant. It was observed that as the ratio of the disperse (Q_d) to continuous phase flow rate (Q_c) increases, the droplet length (L) increases. Figure 3 demonstrates this effect. The reason behind this behavior is the increase in the shearing force of the continuous phase with the increased velocity.

Garstecki et al. [5] correlated experimental results for their T-junction geometry against a scaling law as shown in equation (2). The scaling law relates bubble length (L) to the flow rate ratio, channel width (w) and a dimensionless parameter (α) whose value depends on the geometry. The value of α is typically of order one.

$$\frac{L}{w} = 1 + \alpha \frac{Q_d}{Q_c} \qquad (2)$$

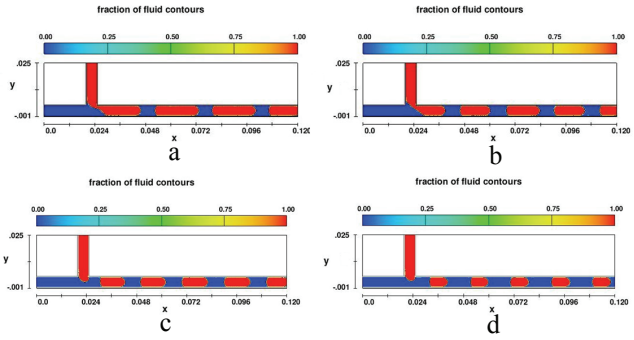

Figure 3: Increase in continuous phase flow rate (Q_c) decreases bubble length. (a: Q_c = 1.8µl/min, b: Q_c = 2.7 µl/min, c: Q_c = 3.6µl/min, d: Q_c = 7.2µl/min) Q_d = 3.9µl/min for all cases.

The results were compared against the scaling law and α for the geometry was found to be 1.48. This has been show in figure 4.

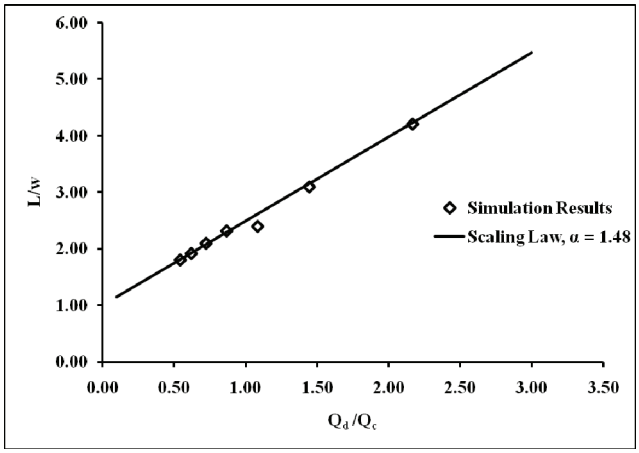

Figure 4: Dependence of L/w ratio on the flow rate ratio.

Finally the bubble formation frequency was calculated for each case and compared against the flow rate ratio (Q_d/Q_c). The bubble formation frequency was found to decrease with an increase in Q_d/Q_c, as shown in figure 5.

3 CO-FLOWING DEVICE

In the co-flowing device, liquid and air enter the micro channel from the same side. They are separated by a barrier. There are two steps in the consequent bubble formation process. First, the gas phase expands downwards

NSTI-Nanotech 2009, www.nsti.org, ISBN 978-1-4398-1784-1 Vol. 3, 2009

and horizontally until a neck is formed, then the neck propagates downstream and its diameter decreases until it finally breaks.

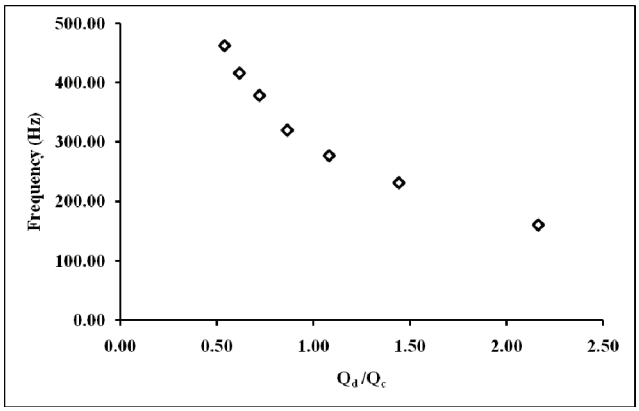

Figure 5: Dependence of bubble formation frequency on flow rate ratios.

3.1 The Setup

Figure 6 describes the general setup for the simulations. The air flows in the region above the separator. The flow rate is represented by Q_g. The region below the separator has liquid flowing with a flow rate of Q_l. The width of the separator is 0.601mm and the depth of the channel is 0.07mm. The height of the channel is 0.691mm. The channel has a length of 20mm.

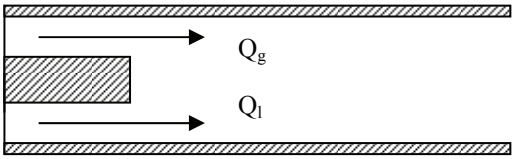

Figure 6: The co-flowing device simulation setup.

3.2 Results and Discussion

To study the breakup process, a case was simulated with air and water flowing together in the device above. The flow rate of air was maintained at 3ml/hour, whereas the flow rate of water (liquid) was maintained at 15ml/hour below the separator. Figure 7 shows the comparison between experimental results [1] and the results obtained from simulation. The simulations show good agreement with the experimental results at all time steps thus validating the **TruVOF**® method.

A scaling law for the size of the discrete fluid segments can be written as [1]:

$$\frac{L}{w} = 1 + \frac{Q_g}{Q_l} \qquad (3)$$

Xiong et al. [1] correlated the experimental data well with the above relation. They also measured the frequency of bubble formation. They compared this data with the analytical expression below:

$$f = \frac{Q_l Q_g}{h^2 w.\left(Q_g + Q_l.\frac{\pi}{4}\right)} \qquad (4)$$

Here f is the frequency of the bubble formation, w is the width of the channel and h is the height of the channel. The bubble formation in the co-flowing device was simulated for a series of different flow rates. Air at flow rates of 2.1, 5.25, 10.5, 21 and 42ml/hour above the separator and water at a fixed flow rate of 21ml/hr below the separator were used. The bubble length was obtained near the exit of the channel when the bubble had reached a steady state. At this stage the bubble occupied the entire channel width due to a high surface tension. The frequency of the bubble formation was also calculated from these simulations. In figure 8 the actual lengths observed for the cases simulated are compared with the values predicted on the basis of the scaling law in equation (3). The frequencies obtained from the simulations were compared with the analytical expression of equation (4) in figure 9.

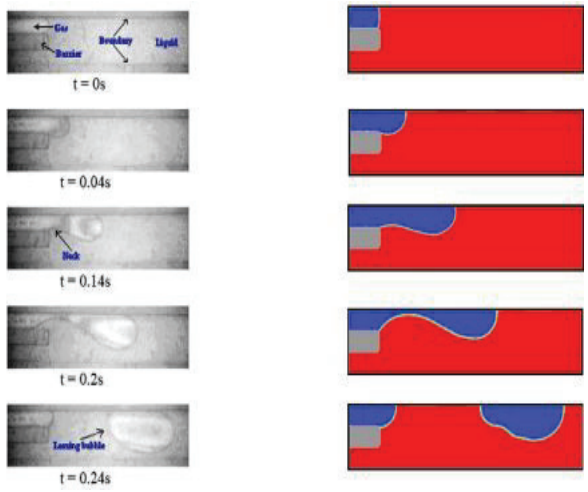

Figure 7: The comparison of experimental results with simulation of bubble formation and breakup process for Q_l =15ml/hr and Q_g = 3ml/hr.

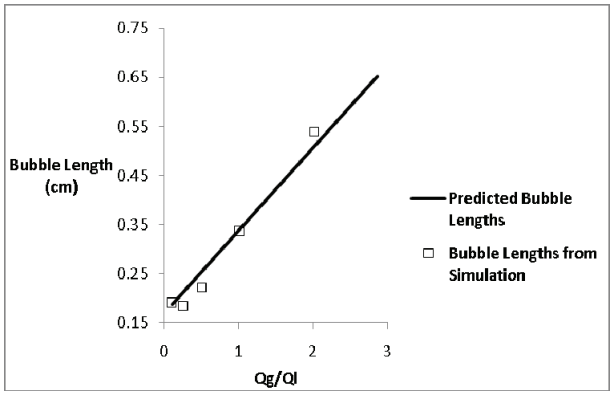

Figure 8: Comparison of the predicted bubble lengths on the basis of the scaling law with bubble lengths observed during the simulation.

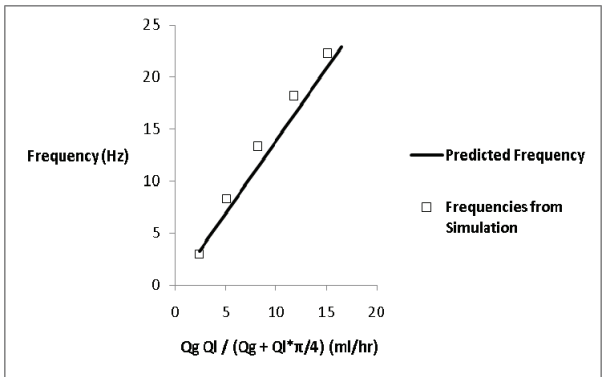

Figure 9: Comparison of the predicted bubble frequencies with the bubble frequencies observed during the simulation.

A higher gas flow rate leads to longer bubbles. This is because with a higher flow rate the gas has a larger force to push the liquid as well as a better ability to resist the liquid pressure at the neck. The simulations showed a good agreement with the scaling law for the bubble length and with the analytical formulation for the frequency.

A qualitative study to determine the effect of viscosity on the size of the bubble generated was also done. The simulations were run with a liquid flow rate of Q_l = 21ml/hour and an air flow rate of Q_g = 2.1ml/hour. The viscosity (μ) of the liquid was changed to simulate different liquids flowing below the separator as follows: Water (μ = 0.92mPas), Water-Glycerol-10% (μ = 1.19mPas), Water-Glycerol-30% (μ = 2.68mPas) and Water-Glycerol-50% (μ = 7.31mPas). The stable bubble size is compared with the experimental results from Xiong et al. [1] in figure 10. The results confirm the general trend observed with respect to the size of the bubbles. As the viscosity increases, the bubble size becomes smaller. This happens because as the thin stream of gas expands to form the bubble, the higher viscous forces counteract the movement, resulting in a smaller bubble.

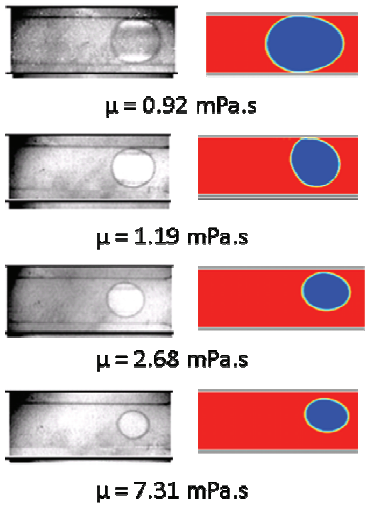

Figure 10: Comparison of experiments with simulation for Q_g = 2.1ml/hour and Q_l = 21ml/hour.

4 ELECTROWETTING

When an electric field is applied across a liquid drop sitting on conductive solid coated with dielectric material, the contact angle of the drop changes. This behavior is called electrowetting. Electrowetting can be used to move, coalesce or split micro-volume droplets.

4.1 Electrowetting simulation

For this example, an electrowetting case for a hemispherical drop of water was chosen. Simulations were run for a 500μm diameter hemispherical drop of water placed on a plate coated with a dielectric material having a dielectric constant of 4.5. The static contact angle of the water drop on the coating is 120° and it has an electrical conductivity of 2.5e-5S/m. A micro-needle electrode is inserted into the top of the drop to apply an electric field across the drop. Figure 11 shows a schematic of the setup.

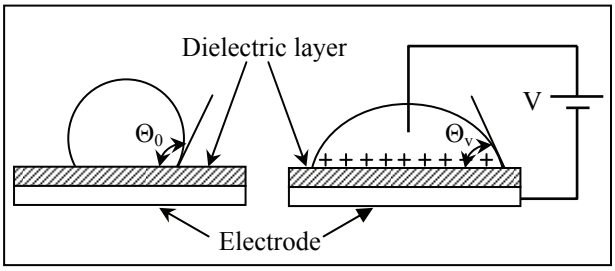

Figure 11: Electrowetting simulation setup.

4.2 Results and discussion

Due to the applied voltage across the droplet, a very thin electric charge layer was observed along the bottom of the droplet as shown in figure 13. This charge layer results in

NSTI-Nanotech 2009, www.nsti.org, ISBN 978-1-4398-1784-1 Vol. 3, 2009

an electric force on the droplet. In addition, a dielectric force also acts on the droplet due to the gradient in the dielectric properties as one moves from the droplet to the surrounding air. These forces make the droplet spread until it reaches a new equilibrium with the surface tension forces.

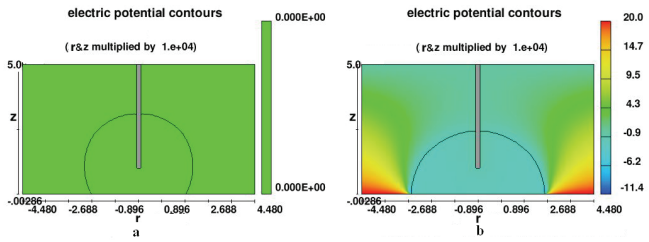

Figure 12: Comparison of drop shape: a: No electric field, b: 20 V electric field. Contours show electric potential.

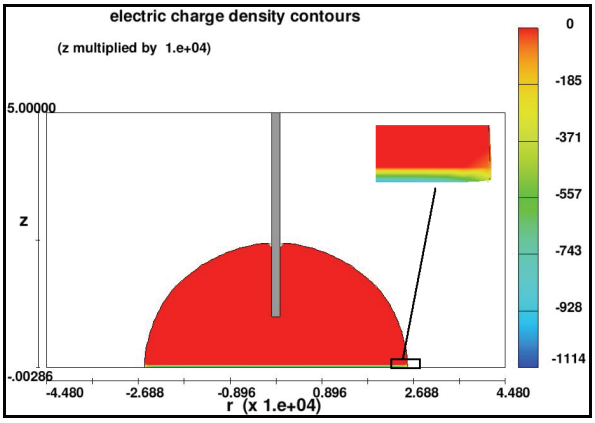

Figure 13: Electric charge density contours for 20 V.

Equation (5) shows the Young-Lippmann equation, which is generally accepted to be reasonably accurate in predicting the change in the apparent contact angle as a function of the applied voltage [6].

$$\cos\theta = \cos\theta_0 + \frac{1}{2\gamma}\frac{\varepsilon\varepsilon_0}{t}V^2 \qquad (5)$$

Equation (5) relates the resulting contact angle (θ) to the applied voltage (V), static contact angle (θ_0), thickness of dielectric layer (t), surface tension coefficient (γ), permittivity of the dielectric layer (ε) and permittivity of vacuum (ε_0). Figure 14 shows a comparison of the simulation results against equation (5) and also against the experimental work done by Cho et al. [6].

Simulation results show a good agreement with the experimental results, except at high voltages where experimental results show a saturation behavior.

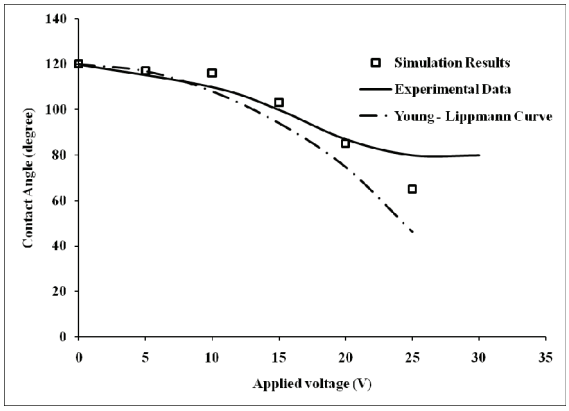

Figure 14: Plot of the apparent contact angle versus applied voltage.

There is no generally accepted theory behind this saturation behavior. This could be due to an instability of the contact line at high voltages or a penetration of electric charge into the dielectric layer at higher voltages [2].

5 CONCLUSIONS

The behavior of a T-junction and a co-flowing device was numerically investigated. For both of them the droplet/bubble formation process was numerically captured and validated against experimental results. Simulation results for both devices were compared against a scaling law for the droplet and bubble length. A simple electrowetting case was also successfully simulated. The results of the electrowetting simulations suggest that as long as the applied voltage is less than the saturation voltage, ***FLOW-3D***® can be used in studying the behavior of electrowetting-based devices. Finally we conclude that **TruVOF**® is suitable for studying and designing droplet-based microfluidic devices.

REFERENCES

[1] R. Xiong, M. Bai and J. Chung, Journal of Micromechanics and Microengineering, 17, 1002-1011, 2007.

[2] F. Mugele and J. Barret, Journal of Physics: Condensed Matter, 17, R705-R774,2005.

[3] C.W. Hirt and B.D. Nichols, J. Comp. Phys., 39, 201-225, 1981.

[4] H. Song, J. D. Tice, and R.F. Ismagilov, Angewandte Chemie International Edition, 42, No.7, 768 - 772, 2003.

[5] P. Garstecki, M.J. Fuerstman, H. A. Stone and G.M.Whitesides, Lab on a Chip, 6, 437–446, 2006.

[6] S.K. Cho, H. Moon and C.J. Kim, J. Microelectromechanical Sys. 12, No. 1, 70-80, 2003.